

Frozen-mode small polaron quantum master equation with variational bound for excitation energy transfer in molecular aggregates

Cite as: J. Chem. Phys. **150**, 224110 (2019); <https://doi.org/10.1063/1.5096287>

Submitted: 15 March 2019 . Accepted: 29 May 2019 . Published Online: 14 June 2019

Hung-Hsuan Teh , Bih-Yaw Jin, and Yuan-Chung Cheng 

COLLECTIONS

Paper published as part of the special topic on [Dynamics of Open Quantum Systems](#)

Note: This paper is part of a JCP Special Topic on Dynamics of Open Quantum Systems.



View Online



Export Citation



CrossMark

ARTICLES YOU MAY BE INTERESTED IN

[A scalable algorithm of numerical real-time path integral for quantum dissipative systems](#)

The Journal of Chemical Physics **150**, 224108 (2019); <https://doi.org/10.1063/1.5100881>

[Density matrix dynamics in twin-formulation: An efficient methodology based on tensor-train representation of reduced equations of motion](#)

The Journal of Chemical Physics **150**, 234102 (2019); <https://doi.org/10.1063/1.5099416>

[Theoretical study of charge carrier transport in organic molecular crystals using the Nakajima-Zwanzig-Mori generalized master equation](#)

The Journal of Chemical Physics **150**, 234101 (2019); <https://doi.org/10.1063/1.5096214>

Lock-in Amplifiers

Find out more today



Zurich
Instruments



Frozen-mode small polaron quantum master equation with variational bound for excitation energy transfer in molecular aggregates

Cite as: J. Chem. Phys. 150, 224110 (2019); doi: 10.1063/1.5096287

Submitted: 15 March 2019 • Accepted: 29 May 2019 •

Published Online: 14 June 2019



View Online



Export Citation



CrossMark

Hung-Hsuan Teh,  Bih-Yaw Jin, and Yuan-Chung Cheng^{a)} 

AFFILIATIONS

Department of Chemistry, National Taiwan University, Taipei City 10617, Taiwan

Note: This paper is part of a JCP Special Topic on Dynamics of Open Quantum Systems.

^{a)} Email: yuanchung@ntu.edu.tw

ABSTRACT

The small polaron quantum master equation (SPQME) is a powerful method for describing quantum dynamics in molecular systems. However, in the slow-bath regime where low-frequency vibrational modes dominate the dynamics, the fully dressed small polaron coordinates lead to errors in the SPQME theory. Furthermore, low-frequency modes also cause infrared divergence in the SPQME method, making the theory applicable only to systems described by spectral densities of the super-Ohmic form. In this study, we propose to treat these low-frequency vibrations as dynamically arrested “frozen” modes in a semiclassical representation and apply the small polaron representation only to the high-frequency vibrations. Furthermore, we show that a variational polaron approach can be utilized to determine the frequency upper bound of the frozen modes, allowing dynamical simulations free of manually tuned parameters. This frozen-mode SPQME is applied to models describing excitation energy transfer (EET) in molecular aggregates and comprehensively compared with the quadiabatic path integral method as well as the Redfield theory to demonstrate the applicability of this new method. We show that errors due to slow baths in the original SPQME theory are significantly reduced by the frozen-mode approximation. More significantly, we show that the new approach successfully extends the SPQME theory to be applicable to systems with the Drude-Lorentz spectral density, resulting in a great expansion of the applicability of the SPQME theory for EET problems. In summary, we demonstrate a “frozen-mode” SPQME that provides efficient and accurate simulations of EET dynamics of molecular systems in a broad parameter regime.

Published under license by AIP Publishing. <https://doi.org/10.1063/1.5096287>

I. INTRODUCTION

Excitation energy transfer (EET) is a fundamental process that plays important roles in many physical and chemical systems, such as conjugated polymers,^{1–3} nanomaterials,⁴ and photosynthetic light-harvesting complexes.^{5–7} Theoretical methods for EET dynamics have drawn much attention in recent years because microscopic details given by theories are critical for the elucidation of factors controlling the EET dynamics and thus device performances in these disordered systems. Thus, comprehensive investigations on characteristics of EET dynamics in molecular systems, such as the multisite structural arrangement^{8–10} and effects of surrounding environments,^{11–13} have been carried out using various

simulation approaches. Furthermore, theories are critical for the interpretation of experimental observations in these complex systems, and it is important to combine theory with experiments to provide molecular details and deeper insights about the mechanism of EET dynamics.

Various numerically exact theoretical methods have been applied to elucidate EET dynamics in condensed-phase molecular systems. Methods such as the path-integral influence functional approaches,¹⁴ density matrix renormalization group,^{15,16} and hierarchy equations of motion (HEOM) method^{17–20} have been employed to successfully simulate EET dynamics in molecular aggregates. In addition, semiclassical methods^{21–23} based on the path integral formalism²⁴ or hybrid approaches^{25–27} also seem to provide

promising results. Nonetheless, these methods are often computationally difficult to apply to large systems, especially in the low-temperature limit.

Therefore, perturbative methods are still widely adopted for EET dynamics. In this regard, methods such as the Redfield theory^{28,29} and the Förster theory³⁰ are still the most popular for describing EET dynamics in molecular aggregates.^{6,12,31–33} The former considers the coupling between a system and its surrounding environments as the perturbation, whereas the latter regards the coupling between different molecules weak enough. Although the two formalisms and their extensions^{34–38} have been successfully utilized to simulate EET dynamics in a large array of systems, one encounters difficulties when dealing with an intermediate regime where the couplings are comparable to each other such that there is no obvious small parameter for perturbation. This regime is often found in the EET dynamics in photosynthetic complex systems,^{31,39} and it hinders the applicable regime of simple perturbative methodologies.

Among the perturbative theories, a second order, time local, small polaron quantum master equation (SPQME) method that provides accurate EET dynamics in a broad parameter space^{40,41} has been developed.^{42–46} Since the SPQME approach yields excellent results in both the Redfield and the Förster limits,^{40,41} it serves as a good starting point to go beyond these two formalisms. However, two key drawbacks still encumber the applicability of the SPQME, namely, that it is applicable only to the super-Ohmic bath and that it fails in the slow-bath regime,^{40,41} both related to low-frequency modes in the bath fluctuations affecting the EET dynamics. Clearly, to improve the performance of the SPQME method, it is required to overcome the shortcomings due to the difficulties in handling the low-frequency bath modes.

In this regard, it is intuitive to consider the low-frequency modes as classical degrees of freedom, while treating the remaining parts quantum mechanically. Theoretical methods that partition bath modes into two portions and then treat them separately with different mechanics have had a long history. For example, in a multilayer theory for quantum dynamics, Wang *et al.*⁴⁷ utilized the mixed quantum-classical Ehrenfest mean-field approach to deal with the low-frequency nuclear motions and applied wave function-based multiconfigurational time-dependent Hartree method to treat the system as well as the high-frequency vibrational modes. Furthermore, the hybrid concept was combined with the noninteracting blip approximation method by Berkelbach *et al.*^{48,49} to simultaneously improve the computational efficiency and retain accuracy of the noninteracting blip method. Their idea was further extended in a paper by Montoya-Castillo *et al.* to improve Redfield theories.⁵⁰ They demonstrated that the applicabilities of Redfield theories can be extended into a highly non-Markovian regime if the low-frequency modes are treated classically. These results have inspired us to propose a hybrid method in the small polaron representation to improve the performance of the SPQME approach.

In this paper, we describe a novel method that combines a classical representation of the low-frequency bath modes with the small polaron representation of the high-frequency bath modes to provide efficient and accurate simulations of EET dynamics in molecular aggregates. A highlight of this work is the determination of the frequency boundary of the low- and high-frequency modes based on

a variational approach, and we show that the frozen-mode approach is related to a crude frequency dependent variational polaron theory. The structure of this paper is described as follows. In Sec. II, we briefly review the small-polaron representation and the corresponding quantum master equation utilized in this study. We emphasize difficulties caused by the low-frequency modes in the SPQME method and then present a semiclassical theory in the small-polaron frame and approximations that incorporate influences of classical slow modes into the SPQME theory. In addition, we further describe the model system employed in this study and additional computational details. In Sec. III, comparisons to the numerically exact quadiabatic path integral (QUAPI) approach^{51,52} with discussions will be furnished, demonstrating that the proposed frozen-mode SPQME yields adequate results even in the slow-bath regime of EET parameters and allows accurate calculations of coherent EET dynamics for systems with Ohmic-type spectral densities.

II. THEORETICAL BACKGROUND

A. Small-polaron transformation

In order to investigate EET dynamics in molecular aggregates, we adopt a system-bath model with a Frenkel exciton system with multiple molecular sites coupled to a harmonic bath ($\hbar = 1$),

$$H = H_s + H_b + H_{sb}, \quad (1)$$

$$H_s = \sum_n \epsilon_n |n\rangle \langle n| + \sum_{n \neq m} J_{nm} |n\rangle \langle m|, \quad (2)$$

$$H_b = \sum_i \omega_i \left(b_i^\dagger b_i + \frac{1}{2} \right), \quad (3)$$

$$H_{sb} = \sum_{n,i} g_{ni} \omega_i |n\rangle \langle n| \left(b_i + b_i^\dagger \right). \quad (4)$$

Here, H_s is the system Hamiltonian, where $|n\rangle$ describes a local excitation at the n th site, the site energy ϵ_n denotes the excitation energy of $|n\rangle$, and J_{nm} is the excitonic coupling between $|n\rangle$ and $|m\rangle$. Environmental effects are included through a harmonic bath Hamiltonian H_b and a bilinear system-bath coupling Hamiltonian H_{sb} , where ω_i and b_i^\dagger (b_i) are the corresponding vibrational frequency and rising (lowering) operator of the i th bath mode, respectively. The harmonic oscillators are diagonally coupled to the multisite system, with a dimensionless exciton-phonon coupling constant g_{ni} describing the coupling between the i th harmonic oscillator and the n th site. To describe the system-bath couplings in the condensed-phase, we assume the bath modes and system-bath couplings are described by spectral density functions $\mathcal{J}_{nm}(\omega)$, which are defined as

$$\mathcal{J}_{nm}(\omega) = \sum_i g_{ni} g_{mi} \omega_i^2 \delta(\omega - \omega_i). \quad (5)$$

Following Jang *et al.*,^{42,44} we transform the total Hamiltonian H into a small polaron frame using a unitary transform $\tilde{H} = e^S H e^{-S}$, where

$$S = - \sum_{n,i} g_{ni} \left(b_i - b_i^\dagger \right) |n\rangle \langle n|. \quad (6)$$

This unitary transformation displaces the nuclear coordinate of each mode i from the electronic ground state vibrational minimum to the excited state vibrational minimum as the n th site is excited. The polaron-transformed Hamiltonian \tilde{H} is then regrouped into three parts,

$$\tilde{H} = H'_s + H'_b + H'_{sb}, \quad (7)$$

$$H'_s = \sum_n \left(\epsilon_n - \sum_i g_{ni}^2 \omega_i \right) |n\rangle\langle n| + \sum_{n \neq m} J_{nm} \langle \theta_n^\dagger \theta_m \rangle |n\rangle\langle m|, \quad (8)$$

$$H'_b = \sum_i \omega_i \left(b_i^\dagger b_i + \frac{1}{2} \right), \quad (9)$$

$$H'_{sb} = \sum_{n \neq m} J_{nm} |n\rangle\langle m| \left(\theta_n^\dagger \theta_m - \langle \theta_n^\dagger \theta_m \rangle \right), \quad (10)$$

where $\langle \cdot \rangle$ represents the thermal average and

$$\theta_n = \exp \left\{ \sum_i g_{ni} \left(b_i - b_i^\dagger \right) \right\} \quad (11)$$

is a bath displacement operator for vibrations on the n th site. $\langle \theta_n^\dagger \theta_m \rangle$ is a temperature-dependent Franck-Condon factor which can be evaluated to yield

$$\langle \theta_n^\dagger \theta_m \rangle = \exp \left\{ \frac{-1}{2} \sum_i (g_{ni} - g_{mi})^2 \coth \left(\frac{\beta \omega_i}{2} \right) \right\}, \quad (12)$$

where we have defined the inverse temperature $\beta = 1/k_B T$. The new system Hamiltonian H'_s includes bath reorganization energies $\lambda_n = \sum_i g_{ni}^2 \omega_i$ and bath-renormalized electronic couplings $J_{nm} \langle \theta_n^\dagger \theta_m \rangle$ because it describes fully dressed polaron states that combine excitons and their polarized environments (displaced oscillators). To retain the coherence effects between the different sites, $J_{nm} \langle \theta_n^\dagger \theta_m \rangle$ is intentionally added to the system part H'_s . In a perturbative treatment, we adopt $H'_0 = H'_s + H'_b$ as the zeroth order Hamiltonian and treat H'_{sb} as the perturbation. In addition, since the Franck-Condon factor $\langle \theta_n^\dagger \theta_m \rangle$ goes to zero both in the strong system-bath coupling and high temperature limits, $J_{nm} \langle \theta_n^\dagger \theta_m \rangle$ also tends to zero in both limits, leading to the dynamical localization in the zeroth-order Hamiltonian.⁵³ Finally, the transformed system-bath couplings in the polaron frame H'_{sb} represent fluctuations of effective electronic couplings around the thermal average $J_{nm} \langle \theta_n^\dagger \theta_m \rangle$, and this form also effectively reduces the magnitude of the polaron-phonon interactions. As a result, the time-dependent second-order perturbative expansion in the polaron frame is more accurate than simple Redfield theories.

B. Small-polaron quantum master equation

In the original SPQME approach, a time-local second order quantum master equation in the polaron representation is employed to derive the reduced dynamics of the polaron states. The resulting equation of motion reads⁴²⁻⁴⁶

$$\begin{aligned} \dot{\sigma} = & -i[H'_s, \sigma(t)] - \int_0^t d\tau \text{Tr}_b \left\{ [H'_{sb}, [H'_{sb}(-\tau), \sigma(t) \rho_b^{\text{eq}}]] \right\} \\ & - i \text{Tr}_b \left\{ [H'_{sb}, e^{-iH'_0 t} (\mathcal{Q} \rho(0)) e^{iH'_0 t}] \right\} \\ & - \int_0^t d\tau \text{Tr}_b \left\{ [H'_{sb}, [H'_{sb}(\tau - t), e^{-iH'_0 t} (\mathcal{Q} \rho(0)) e^{iH'_0 t}]] \right\}, \quad (13) \end{aligned}$$

where $\text{Tr}_b \{ \cdot \}$ denotes the trace over all bath degrees of freedom, $\sigma(t) = \text{Tr}_b \{ \rho(t) \}$ is the reduced density matrix of the excitonic system, and $\rho_b^{\text{eq}} = e^{-\beta H'_b} / \text{Tr}_b \{ e^{-\beta H'_b} \}$ is the thermalized density matrix of the bath. In addition, $H'_{sb}(t) = e^{iH'_0 t} H'_{sb} e^{-iH'_0 t}$, where $H'_0 = H'_s + H'_b$ is the zeroth-order Hamiltonian. $\mathcal{Q} = 1 - \mathcal{P}$ is the complementary part of a projection operator defined by $\mathcal{P} = \rho_b^{\text{eq}} \text{Tr}_b \{ \cdot \}$.

The first term in Eq. (13) describes the coherent dynamics of the polaron system, the second term characterizes the dissipative dynamics induced by the system-bath couplings, and the last two terms are inhomogeneous terms describing dynamics of polaron formation. The inhomogeneous terms go to zero rapidly as the total system reaches equilibrium. In this study, we assume that the bath relaxation following the vertical excitation is extremely fast such that we can neglect the inhomogeneous terms. This approximation is valid especially in simulating EET dynamics of molecular aggregates since the bath relaxation normally takes place in a much shorter time scale compared to the time scale of the system dynamics.⁵³

Previous studies have demonstrated that the SPQME approach, which imposes fully dressed polaron coordinates, provides excellent results in a wide range of parameters. However, in the slow-bath regime, the small polaron method does not yield good results.^{40,53} Moreover, when the Ohmic bath is used in the small polaron theory, the thermally averaged Franck-Condon factor $\langle \theta_n^\dagger \theta_m \rangle$ becomes zero, which makes the theory unable to describe coherent dynamics in Ohmic bath systems.⁵⁴ In addition, the expansion of the dissipation term in Eq. (13) includes time correlation functions comprising integral kernels that diverge at the low-frequency regime if the bath spectral density is of an Ohmic form. This is an infrared divergence. Spectral densities such as the Drude-Lorentz spectral density, however, are widely and successfully utilized for theoretical analysis of experimental results for many EET systems. As a result, a generalized SPQME that can circumvent the problems caused by the low-frequency modes will be highly desirable.

C. Frozen-mode small-polaron quantum master equation

Since at a finite temperature, the low-frequency modes behave more classically than the high-frequency vibrations, we seek to separate them from the remaining system and describe them from a classical point of view, while leaving high-frequency modes to be treated within the SPQME framework. In order to obtain the classical correspondence of the low-frequency modes, we apply the partial Wigner transform over the low-frequency degrees of freedom. The Hamiltonian in Eq. (1) can be recast as

$$\begin{aligned} H^W(\mathbf{P}_{\text{low}}, \mathbf{Q}_{\text{low}}) = & \sum_n \epsilon_n |n\rangle\langle n| + \sum_{n \neq m} J_{nm} |n\rangle\langle m| + \sum_{i \in \text{high}} \omega_i \left(b_i^\dagger b_i + \frac{1}{2} \right) \\ & + \sum_{n, i \in \text{high}} g_{ni} \omega_i |n\rangle\langle n| \left(b_i + b_i^\dagger \right) + \sum_{i \in \text{low}} \frac{1}{2} \omega_i (P_i^2 + Q_i^2) \\ & + \sum_{n, i \in \text{low}} \sqrt{2} g_{ni} \omega_i Q_i |n\rangle\langle n|, \quad (14) \end{aligned}$$

where the subscript low (high) denotes the low-frequency (high-frequency) modes, the superscript W represents the partial Wigner

transform over the low-frequency modes, and P_i and Q_i are the classical momentum and position of the i th mode, respectively. In this representation, the corresponding expectation value for a Hermitian operator O is calculated from

$$\langle O \rangle = \text{Tr} \left\{ \int d\mathbf{P}_{\text{low}} \int d\mathbf{Q}_{\text{low}} \rho^{\text{W}}(\mathbf{P}_{\text{low}}, \mathbf{Q}_{\text{low}}, t) O^{\text{W}}(\mathbf{P}_{\text{low}}, \mathbf{Q}_{\text{low}}) \right\}. \quad (15)$$

Note that ρ^{W} and O^{W} are operators in the excitonic plus high-frequency vibrational Hilbert space, and the trace is taken over all these fast degrees of freedom.

The partial Wigner transform over slow degrees of freedom provides rigorous semiclassical representation of quantum systems. Various hybrid approaches have been developed in this representation, such as the mixed quantum-classical Liouville dynamics^{25–27} and the reduced density matrix hybrid approach.^{48,49} There, a semiclassical approximation is often applied, and the transformed degrees of freedom are then propagated by the classical Hamilton's equations. However, the interactions between the quantum and the classical regions often lead to difficulties of hybrid approaches, and the description of feedbacks from the quantum degrees of freedom to the classical degrees of freedom often leads to high computational cost. Therefore, applications of semiclassical methods are highly nontrivial, and their applicabilities must be examined for each particular physical problem.

In a recent study, Montoya-Castillo *et al.* demonstrated that by treating low-frequency modes classically, the applicabilities of Redfield theories can be extended into highly non-Markovian regime.⁵⁰ In their work, two different treatments of the classical modes were examined. They first tested a frozen-mode approximation that has the low-frequency modes “frozen” in the initial phase space points $(\mathbf{P}_{\text{low}}^0, \mathbf{Q}_{\text{low}}^0)$ sampled from the thermalized distribution, and then, they relaxed this approximation and allowed the high-frequency modes to be evolved in the mean field of the low-frequency modes that are propagated based on Newtonian dynamics. Nonetheless, they have demonstrated that the frozen-mode approximation yields excellent results, and the dynamical treatment of the classical slow modes exhibits a much higher computational cost yet only a slight improvement of the results. Hence, in this study, we focus on the frozen mode approximation. Since we aim to treat the remaining high-frequency degrees of freedom with the SPQME theory, we apply the polaron transformation to the high-frequency modes to reach the polaron-transformed Hamiltonian in the partial Wigner representation

$$\begin{aligned} \widetilde{H}^{\text{W}}(\mathbf{P}_{\text{low}}^0, \mathbf{Q}_{\text{low}}^0) = & \sum_n \left(\epsilon_n - \sum_{i \in \text{high}} g_{ni}^2 \omega_i + \Delta \epsilon_n(\mathbf{P}_{\text{low}}^0, \mathbf{Q}_{\text{low}}^0) \right) |n\rangle \langle n| \\ & + \sum_{i \in \text{high}} \omega_i \left(b_i^\dagger b_i + \frac{1}{2} \right) + \sum_{n \neq m} J_{nm} |n\rangle \langle m| \theta_n^\dagger \theta_m, \end{aligned} \quad (16)$$

where the influence of the low-frequency modes in Eq. (14) becomes static energy disorders in the renormalized site energies,

$$\Delta \epsilon_n(\mathbf{P}_{\text{low}}^0, \mathbf{Q}_{\text{low}}^0) = \sum_{i \in \text{low}} \omega_i \left[\frac{(P_i^0)^2 + (Q_i^0)^2}{2} + g_{ni} \sqrt{2} Q_i^0 \right]. \quad (17)$$

In addition, the expectation value in Eq. (15) is significantly simplified,

$$\langle O \rangle \simeq \text{Tr} \left\{ \int d\mathbf{P}_{\text{low}}^0 \int d\mathbf{Q}_{\text{low}}^0 \rho^{\text{W}}(\mathbf{P}_{\text{low}}^0, \mathbf{Q}_{\text{low}}^0, 0) O^{\text{W}}(\mathbf{P}_{\text{low}}^0, \mathbf{Q}_{\text{low}}^0) \right\}, \quad (18)$$

which can be calculated straightforwardly by Monte Carlo sampling over the initial Wigner distribution $\rho^{\text{W}}(\mathbf{P}_{\text{low}}^0, \mathbf{Q}_{\text{low}}^0, 0)$. Note that if the initial bath modes are in thermal equilibrium described by the density matrix, ρ_b^{eq} , the partial Wigner transform over the low-frequency modes in Eq. (18) results in a multivariate distribution calculated from a multiplication of independent normal distributions $\mathcal{N}(x; x_0, \sigma) = \frac{1}{\sqrt{2\pi\sigma}} e^{-(x-x_0)^2/2\sigma^2}$ with zero mean and standard deviation σ_i for the classical momentum (P_i) and position (Q_i) of each low-frequency mode ($i \in \text{low}$),

$$(\rho_{b,\text{low}}^{\text{eq}})^{\text{W}}(\mathbf{P}_{\text{low}}^0, \mathbf{Q}_{\text{low}}^0) = \prod_{n \in \text{low}} \mathcal{N}(P_i^0; 0, \sigma_i) \mathcal{N}(Q_i^0; 0, \sigma_i), \quad (19)$$

where

$$\sigma_i = \sqrt{\frac{1}{2 \tanh(\omega_i \beta / 2)}}. \quad (20)$$

Equation (19) leads to efficient samplings for calculating expectation values [Eq. (18)]. Note that the reduced dynamics given by the polaron-transformed Hamiltonian in the partial Wigner representation follows the same SPQME using the spectral density of the high-frequency modes. Therefore, an average over static disorder caused by the frozen low-frequency modes will recover the full dynamics.

Moreover, the separation of bath modes into a high-frequency part and a low-frequency part can be achieved by introducing a splitting term, $\mathcal{S}(\omega)$, defined by^{48,49}

$$\mathcal{S}(\omega) = \begin{cases} [1 - (\omega/\omega_s)^2]^2, & \omega \leq \omega_s, \\ 0, & \omega > \omega_s. \end{cases} \quad (21)$$

Here, ω_s is the splitting frequency that separates the low-frequency part from the high-frequency part, and it is an adjustable parameter which will be determined from a physical point of view later. We multiply $\mathcal{S}(\omega)$ onto the original spectral density of the system to yield two spectral densities mainly consisted of low-frequency modes and high-frequency modes, respectively,

$$\mathcal{J}_{nm,\text{low}}(\omega) = \mathcal{S}(\omega) \mathcal{J}_{nm}(\omega), \quad (22)$$

$$\mathcal{J}_{nm,\text{high}}(\omega) = (1 - \mathcal{S}(\omega)) \mathcal{J}_{nm}(\omega). \quad (23)$$

Clearly, $\mathcal{J}_{nm}(\omega) = \mathcal{J}_{nm,\text{low}}(\omega) + \mathcal{J}_{nm,\text{high}}(\omega)$ is preserved. Note that when $\omega_s = 0$, all bath modes are addressed with the small-polaron transformation and no frozen mode exists, and this recovers the original SPQME method. On the other hand, in the $\omega_s = \infty$ limit, all modes will be treated statically and classically, and no polaron transformation will be applied [Eq. (14)]. As a result, the excitation will propagate on the static potential energy surface caused by the frozen modes, which reduces to pure adiabatic dynamics. It is interesting to note that theoretical analysis of Redfield theory⁵⁰ and non-interacting blip approximation method⁴⁸ in the $\omega_s = \infty$ limit were

carried out for two-level systems previously, and both methods also reduce to adiabatic dynamics in the limit. Furthermore, the splitting function in Eq. (23), $(1 - \mathcal{S})$, exhibits an ω^4 frequency dependence in the low-frequency regime; hence, the divergence problem in the SPQME can be avoided, allowing the SPQME to be applied to systems whose spectral density has an Ohmic form. We will show that our frozen-mode small polaron-quantum master equation (FM-SPQME) method is applicable to the Drude-Lorentz spectral density, without numerical difficulties due to the infrared divergence.

D. Variational determination of the splitting frequency

At this point, we shall have a discussion on the justification of the frozen-mode approach in the variational polaron framework and a proposal to determine the splitting frequency without manually tunable parameters. In this work, the fully dressed small polaron basis is adopted to perturbatively determine the excitation energy transfer dynamics in molecular aggregates. However, it is also well known that the strengths of electronic couplings, exciton-phonon couplings, and temperature are all significant factors that influence the degree of polaronic interactions, and a variational polaron ansatz with variational parameters determining the degree of polaronic dressing would provide much more accurate results.^{55–58} As a result, the variational polaron approach has been developed to accurately treat EET dynamics in molecular aggregates and photosynthetic systems without the shortcomings of the small polaron method.^{40,54,59–61}

In this work, instead of adopting the variational polaron approaches that exhibit much more complicated equations of motion, we use a variational ansatz to determine the splitting frequency for the frozen-mode. The frozen-mode method is justified by the observation that the degree of polaronic dressing also depends on the frequency of the phonon mode. In this regard, our frozen-mode method can be considered as a crude variational polaron theory with step-function frequency-dependent polaronic dressing coefficient, plus a semiclassical treatment to the low-frequency slow dynamics. The crude step-function ansatz is justified by the sharp polaron transition shown in numerical calculations of polaronic effects.^{57,58}

To determine the splitting frequency based on a variational polaron method, we adopt the theory with a single dressing coefficient described by Cheng and Silbey.⁵⁸ In the theory, the electronic system is coupled to a selected vibrational mode to each site, and a partial polaron transformation is considered,

$$U = e^{-\sum_n f_n (b_n - b_n^\dagger)} |n\rangle \langle n|, \quad (24)$$

where f_n is a real number between 0 and g_n that we termed the dressing coefficient. The $f_n = 0$ limit corresponds to the bare exciton basis, and the $f_n = g_n$ limit recovers the small polaron theory. To determine the value of f_n variationally, we focus on a dimer system,

$$H_s = \Delta \sigma_z + J_0 \sigma_x, \quad (25)$$

where each site is coupled to an identical and independent vibrational mode with frequency ω . In this case, the upper bound of the free energy can be expressed as a function of the dressing

coefficient,⁵⁸

$$A = \sum_n \omega f_n (f_n - 2g_n) - \beta^{-1} \ln \left\{ \text{Tr} \left[e^{-\beta(\Delta \sigma_z + J_{\text{eff}} \sigma_x)} \right] \right\}, \quad (26)$$

where the dressed excitonic coupling reads

$$J_{\text{eff}} = J_0 \cdot \exp \left\{ - \sum_n J_n^2 \coth \left(\frac{\beta \omega_n}{2} \right) \right\}. \quad (27)$$

In order to minimize A with respect to f_n , we consider solving $\partial A / \partial f_k = 0$. It turns out that

$$f_n / g_n = \left\{ 1 + \tanh \left(\beta \sqrt{\Delta^2 + (J_{\text{eff}})^2} \right) \frac{(J_{\text{eff}})^2 \coth(\beta \omega / 2)}{\omega \sqrt{\Delta^2 + (J_{\text{eff}})^2}} \right\}^{-1}. \quad (28)$$

Note that the dressing ratio $f_n / g_n \rightarrow 1$ as $\omega \rightarrow \infty$, and $f_n / g_n \rightarrow 0$ as $\omega \rightarrow 0$. Therefore, the variational theory predicts that the degree of optimal polaronic dressing is dependent on the mode frequency. Low frequency modes tend to be weakly dressed, and high frequency modes tend to be strongly dressed. This clearly justified the frequency-dependent treatment of exciton-phonon dynamics proposed in this paper. Numerical determination of the optimal f_n / g_n in a broad parameter regime shows that its value changes sharply from almost zero to 1 as a function of ω at a certain frequency,⁵⁸ which shall correspond to the splitting frequency described in this work. As a result, it is reasonable to set our splitting frequency ω_s at the point $f_n / g_n = 1/2$, which leads to

$$\frac{\omega_s}{\coth(\beta \omega_s / 2)} = \frac{(J_{\text{eff}})^2 \tanh \left(\beta \sqrt{\Delta^2 + (J_{\text{eff}})^2} \right)}{\sqrt{\Delta^2 + (J_{\text{eff}})^2}}, \quad (29)$$

and J_{eff} can now be generalized to a set of continuous modes,

$$J_{\text{eff}} = J_0 e^{-\sum_n \left(\frac{g_n}{2} \right)^2 \coth \left(\frac{\beta \omega_n}{2} \right)} \quad (30)$$

$$= J_0 e^{-\int_{\omega_s}^{\infty} d\omega \mathcal{J}(\omega) \frac{1}{\omega^2} \coth \left(\frac{\beta \omega}{2} \right)}. \quad (31)$$

Equations (29) and (31) allow us to determine the splitting frequency from Δ , J_0 , and β . Note that this variationally determined splitting frequency also considers the temperature effect on ω_s . Moreover, in the low temperature limit,

$$\omega_s = \frac{(J_{\text{eff}})^2}{\sqrt{\Delta^2 + (J_{\text{eff}})^2}}, \quad (32)$$

whereas in the high temperature limit,

$$\omega_s = \sqrt{2(J_{\text{eff}})^2}. \quad (33)$$

E. Bath discretization and frozen-mode sampling

Given a spectral density $\mathcal{J}_{nm}(\omega)$ and a splitting frequency ω_s , the spectral density of the low-frequency modes can be determined [Eq. (22)]. However, since the resulting $\mathcal{J}_{nm,\text{low}}(\omega)$ is a continuous function, a discretized correspondence of classical modes to $\mathcal{J}_{nm,\text{low}}(\omega)$ is required in order to treat the low-frequency vibrations classically. To this end, we follow a procedure of bath discretization proposed by Wang *et al.*⁶² To describe the continuous $\mathcal{J}_{nm}(\omega)$ using N_{low} harmonic modes, we assume that the density

of state, $W(\omega)$, of the low-frequency modes has the mathematical form

$$W(\omega) = a \frac{\mathcal{J}_{nm,low}(\omega)}{\omega}, \quad (34)$$

where a is a normalization constant. The functional form of $W(\omega)$ is not important as long as in the calculations N_{low} is large enough. Nevertheless, different choices of the functional form may result in different rates of convergence. The density of states must satisfy two physical conditions, namely, the normalization to a total of N_{low} modes,

$$\int_0^{\infty} W(\omega) d\omega = N_{low}, \quad (35)$$

and a proper frequency assigned to the k th mode,

$$\int_0^{\omega_k} W(\omega) d\omega = k, \quad (36)$$

where $k = 1, 2, \dots, N_{low}$ is the mode index. Given these two conditions, the normalization factor a can be obtained from Eq. (35), and the sampled frequency ω_k can be determined from Eq. (36). In addition, the coupling constant g_{nk} between the n th site and the k th low-frequency mode can be determined from the definition of the spectral density [Eq. (5)], resulting in

$$g_{nk}g_{mk} = \frac{\mathcal{J}_{nm}(\omega_k)}{\omega_k^2 W(\omega_k)}. \quad (37)$$

In summary, we propose a frozen-mode small-polaron quantum master equation (FM-SPQME) method that amounts to running SPQME dynamics with disordered Hamiltonian given by static disorders calculated from positions and momenta sampled from equilibrium Wigner distribution of frozen low-frequency modes. The FM-SPQME propagates reduced dynamics in the small-polaron frame based on the polaron-transformed Hamiltonian in the partial Wigner representation [Eq. (16)] and the spectral density of the high-frequency modes [Eq. (23)], while the influences of the slow vibrational modes are included by averaging over an ensemble of trajectories with static energetic disorders sampled from the equilibrium Wigner distribution of the low-frequency vibrations [Eq. (22)]. In our investigation over a wide range of parameters, 200 low-frequency modes and 200 trajectories for the sampling are sufficient to achieve excellent convergence. As a result, the FM-SPQME approach is computationally efficient, and this excellent convergence property is attained by the proper choice of the functional form of the density of states as well as the frozen-mode approximation. Note that the current formalism can be directly generalized to achieve a hybrid quantum-classical method that incorporates classical dynamics of the slow modes to go beyond the frozen-mode approximation. Nevertheless, the consideration of classical dynamics in a hybrid quantum-classical approach often leads to rapid oscillations in quantum phase factors, and the required number of trajectories for obtaining an accurate ensemble average often increases rapidly as a function of the evolution time. As a result, long-time dynamics in a hybrid quantum-classical method often suffer from convergence problems. By contrast, methods with the frozen-mode approximation cleverly avoid the demand of myriad sampling of trajectories.

III. RESULTS AND DISCUSSIONS

To investigate the applicability of the FM-SPQME method for coherent energy transfer in molecular aggregates, we first study EET dynamics in a model dimer system. This simple model system allows us to fully explore the applicable parameter space and the effectiveness of the frozen-mode approximation.

We adopt the following dimer exciton Hamiltonian:

$$H_s = \Delta\sigma_z + J\sigma_x, \quad (38)$$

where σ_z and σ_x are the Pauli matrices, 2Δ is the site energy gap, and J represents the excitonic coupling between the two sites. For simplicity, we assume that the two sites are coupled to identical independent harmonic baths in this study, i.e., $\mathcal{J}_{nm}(\omega) = \mathcal{J}(\omega)\delta_{nm}$. The initial condition is considered as a product state,

$$\rho(0) = |1\rangle\langle 1| \otimes \rho_b^{\text{eq}}, \quad (39)$$

with the system initially excited at site 1 and the bath in thermal equilibrium.

A. Super-Ohmic spectral density

In this section, we provide comparisons between the FM-SPQME method and the quasiadiabatic path integral (QUAPI) approach^{51,52} for a model system described by a super-Ohmic spectral density,

$$\mathcal{J}_{so}(\omega) = \gamma \frac{\omega^3}{\omega_c^2} e^{-\omega/\omega_c}, \quad (40)$$

where γ is the exciton-phonon coupling strength and ω_c is the bath cut-off frequency. We aim to investigate the applicable regime of the FM-SPQME and examine its performance in the slow-bath limit. The QUAPI data were published previously.⁴¹ For the numerical scheme of QUAPI, the method detailed in Refs. 52 and 63 was used. The numerical calculation is based upon the symmetric Trotter splitting of short time propagators, and the sizes of the time slice and memory-time window critically affect the accuracy of the results, especially for dynamics with slow bath modes and long memory times. In all the QUAPI calculations, the time slice is gradually reduced and memory-time window is gradually enlarged for each parameter set individually to ensure convergence.

A key parameter in the FM-SPQME method is the splitting frequency ω_s that divides the bath modes into the low- and high-frequency parts. In order to examine the choices of ω_s , we compare population dynamics calculated using the FM-SPQME with different values of ω_s to dynamics obtained from the numerically exact QUAPI method in a slow-bath regime ($J/\omega_c > 1$) (Fig. 1). As the fully dressed coordinates are not a proper representation in this regime, it is no surprise that the SPQME significantly overestimates the decoherence rate. By contrast, we observe that the FM-SPQME dynamics gradually approach the exact result with a change in ω_s from 0 to J . From previous studies,^{40,53} we know that the ratio of the fundamental frequency of the system dynamics to the bath dynamics, J/ω_c , gauges the performance of the small polaron method. Note that the variationally determined splitting frequency ω_s is also close to J in this strong excitonic coupling and low temperature limit [Eq. (32)]. Moreover, Fig. 1 shows that when ω_s is too large, FM-SPQME no longer yields accurate dynamics because too many bath modes are

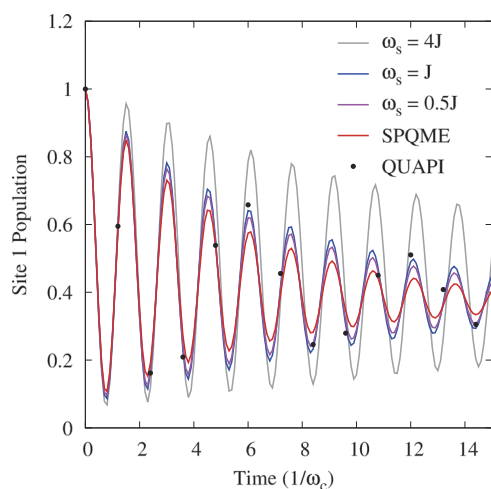


FIG. 1. Population dynamics simulated by the FM-SPQME (lines) and QUAPI (black dots) in a strong excitonic coupling regime ($J/\omega_c = 2.0$). We examine the effects of different values of splitting frequency ω_s . Other parameters are $\Delta/\omega_c = 0.5$, $\gamma = 0.2/\pi$, and $\beta\omega_c = 2.0$.

considered frozen. In the calculations for the Ohmic system presented in the following, we employ variationally determined ω_s as our standard splitting frequency for the FM-SPQME method.

Figure 2 shows population dynamics simulated by the FM-SPQME and those by the QUAPI method for systems in the weak excitonic coupling regime ($J/\omega_c = 0.5$) with different system-bath coupling strengths. This weak excitonic coupling case is a parameter regime in which the SPQME yields excellent results because the dynamics of the bath is faster than that of the system. Note that the FM-SPQME method also yields excellent results even with a sizable splitting frequency, ω_s , in which a significant portion of vibrational harmonics is treated as frozen modes. This excellent performance of the FM-SPQME indicates that the frozen-mode

approximation does capture the essential physics of the dynamically arrested low-frequency motions. Moreover, the FM-SPQME method yields accurate results in the incoherent Förster limit [Fig. 2(c)]. We conclude that at this weak excitonic coupling regime, the frozen-mode approximation with variationally determined ω_s does not affect the quality of the SPQME results across a broad range of system-bath coupling strengths.

On the other hand, in Fig. 3, we benchmark the performance of the FM-SPQME method in a strong excitonic coupling regime ($J/\omega_c = 2.0$). This is a case in which the bath dynamics is much slower than the EET dynamics. Noticeably, SPQME fails to describe the decoherence time of the system even at the weak system-bath coupling strength ($\gamma = 0.2/\pi$) [Fig. 3(a)]. Clearly, the small polaron frame does not provide a suitable representation in this limit because the system dynamics is so fast that the harmonic modes do not have sufficient time to respond accordingly. By contrast, with the frozen-mode treatment for the low-frequency modes, the FM-SPQME leads to much better agreement with the profile of the QUAPI results. The Rabi frequency looks wrong, but this is mostly due to the undersampling of the QUAPI data points. In the weak system-bath coupling limit shown in Fig. 3, we estimate a bare exciton energy gap of about $4.12\omega_c$, corresponding to a period of about $1.53/\omega_c$, which is close to the FM-SPQME results. Moreover, as the system-bath coupling strength γ increases, the system is more strongly influenced by the phonons. Therefore, the population dynamics of trajectories sampled in the FM-SPQME calculation gradually become incoherent transfer and the ensemble average provides an accurate description, as shown in Fig. 3(c).

In Fig. 4, we investigate temperature effects on the performance of the FM-SPQME method for a model system in the intermediate coupling regime. We observe that the FM-SPQME provides improved results over simple SPQME across the whole temperature range studied in this work. Also, it is insightful to note the temperature dependence of the performance of the small-polaron approach here. At high temperatures [Fig. 4(c)], the system is strongly scattered by the thermal bath, causing the system to localize dynamically on the two sites. The situation is similar to the case of weak excitonic

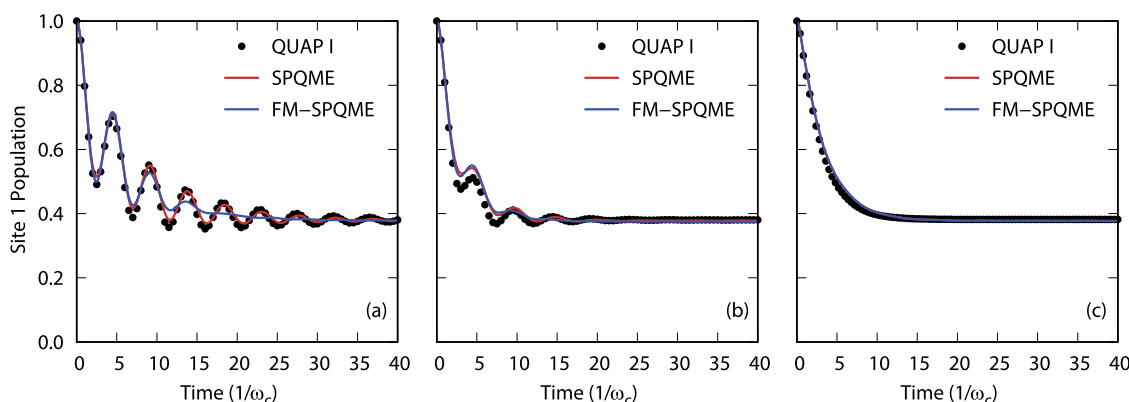


FIG. 2. Population dynamics simulated by the SPQME (red line), the FM-SPQME (blue line), and the QUAPI (black dots) in a weak excitonic coupling regime ($J/\omega_c = 0.5$) with different values of system-bath coupling strengths: (a) $\gamma = 0.2/\pi$, (b) $\gamma = 0.5/\pi$, (c) $\gamma = 2.0/\pi$. Other parameters are $\Delta/\omega_c = 0.5$ and $\beta\omega_c = 0.5$. FM-SPQME splitting frequencies are (a) $\omega_s/\omega_c = 0.60$, (b) $\omega_s/\omega_c = 0.45$, (c) $\omega_s/\omega_c = 0.057$.

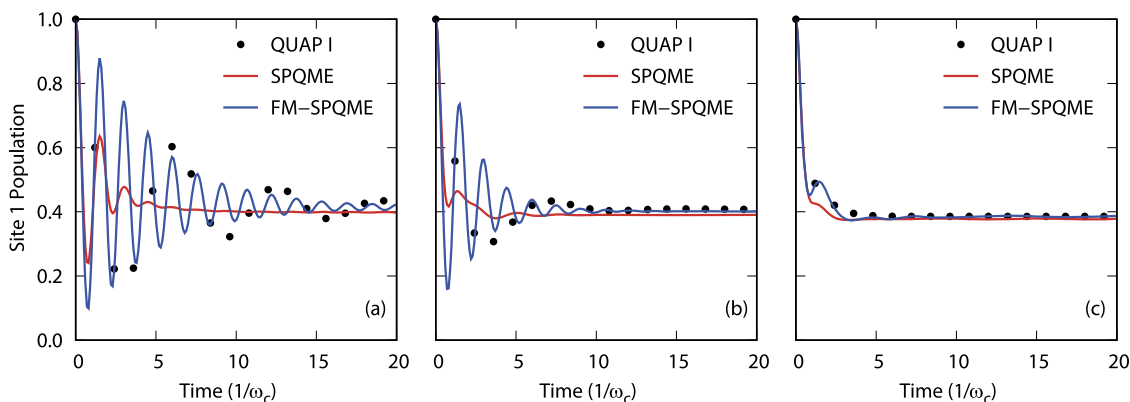


FIG. 3. Population dynamics simulated by the SPQME (red line), the FM-SPQME (blue line), and the QUAPI (black dots) in a strong excitonic coupling regime ($J = 2.0\omega_c$) with different values of system-bath coupling strengths: (a) $\gamma = 0.2/\pi$, (b) $\gamma = 0.5/\pi$, (c) $\gamma = 2.0/\pi$. Other parameters are $\Delta/\omega_c = 0.5$ and $\beta\omega_c = 0.5$. FM-SPQME splitting frequencies are (a) $\omega_s/\omega_c = 2.56$, (b) $\omega_s/\omega_c = 2.46$, (c) $\omega_s/\omega_c = 0.86$.

coupling, and polaron-based methods are expected to be suitable in this regime. On the other hand, the quality of the SPQME dynamics deteriorated when going from the low temperature [Fig. 4(a)] to the intermediate temperature [Fig. 4(b)]. This observation can be explained by the variance of the perturbation term in the small polaron frame,

$$\text{Tr}_b\{H_{sb}^2 \rho_b^{\text{eq}}\} = J^2(1 - \langle \theta_1^\dagger \theta_2 \rangle^2), \quad (41)$$

where the Franck-Codon factor ($\langle \theta_1^\dagger \theta_2 \rangle$) is given in Eq. (12). Note that the Franck-Codon factor is temperature dependent, and it decreases as temperature increases due to thermal population of the phonon modes. Hence, in the low temperature case, the variance increases as the temperature increases, which leads to the slight deviation of the SPQME results from the exact results in Fig. 4(b). Interestingly, by treating the more populated low-frequency modes using the classical

approximation, the FM-SPQME reduces the variance of the perturbation term and clearly improves the results at the intermediate temperature.

In summary, it is clear that the FM-SPQME yields improved results over the SPQME method when the slow modes dominate the dynamics. This frozen-mode approximation is well founded physically. In the parameter regime investigated in this work, the frozen-mode approximation does not reduce the quality of the results. Note that this is no surprise since the super-Ohmic spectral density is predominated by high-frequency vibrations.

B. Drude-Lorentz spectral density

In order to confirm that the FM-SPQME is not restricted to the super-Ohmic spectral density, we apply the method to simulate the EET dynamics in a model system with the Drude-Lorentz

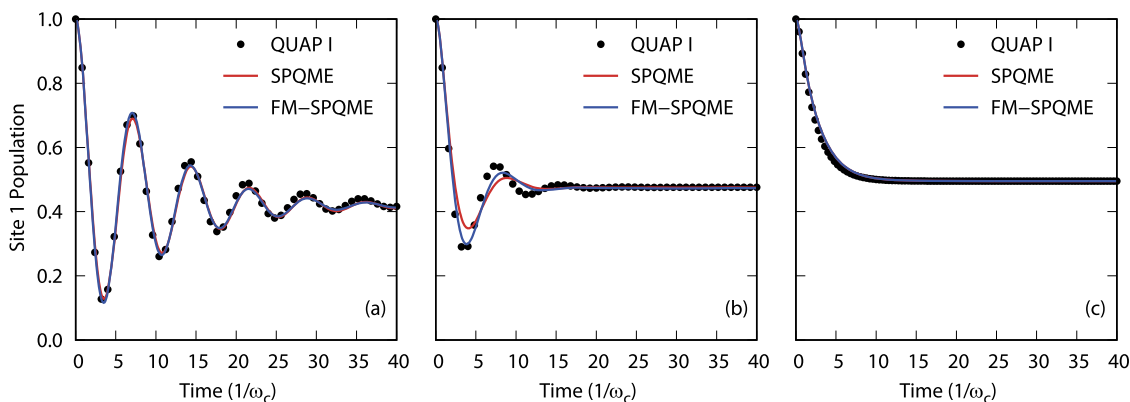


FIG. 4. Population dynamics simulated by the SPQME (red line), the FM-SPQME (blue line), and the QUAPI (black dots) at different values of inverse temperatures: (a) $\beta\omega_c = 2.0$, (b) $\beta\omega_c = 0.5$, (c) $\beta\omega_c = 0.1$. Other parameters are $\Delta/\omega_c = 0.1$, $J/\omega_c = 0.5$, and $\gamma = 0.5/\pi$. FM-SPQME splitting frequencies are (a) $\omega_s/\omega_c = 0.57$, (b) $\omega_s/\omega_c = 0.46$, (c) $\omega_s/\omega_c = 0.032$.

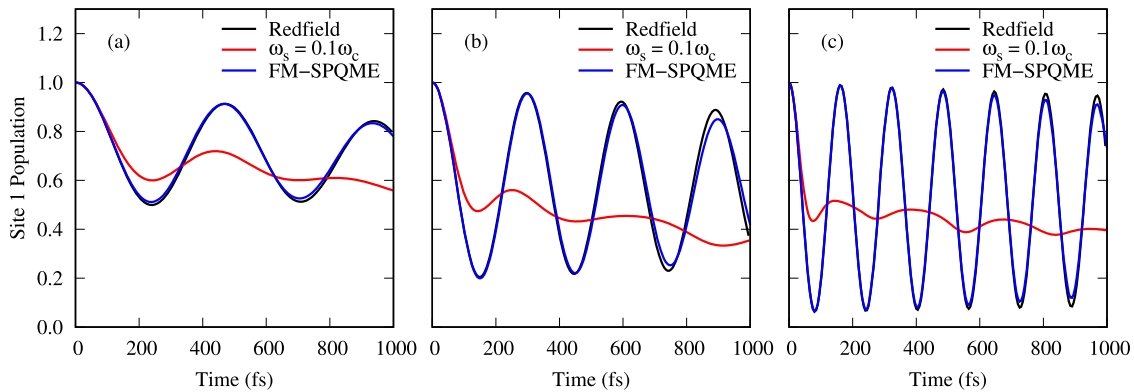


FIG. 5. Population dynamics simulated by the FM-SPQME method and the Redfield theory at a low temperature ($T = 77$ K) with different values of excitonic couplings: (a) $J = 25$ cm^{-1} , (b) $J = 50$ cm^{-1} , (c) $J = 100$ cm^{-1} . Other parameters are $\lambda = 1$ cm^{-1} , $\Delta = 25$ cm^{-1} , and $\omega_c = 50$ cm^{-1} . FM-SPQME splitting frequencies are (a) $\omega_s/\omega_c = 0.60$, (b) $\omega_s/\omega_c = 1.20$, (c) $\omega_s/\omega_c = 2.19$.

spectral density,

$$\mathcal{J}_{\text{DL}}(\omega) = 2\lambda \frac{\omega\omega_c}{\omega^2 + \omega_c^2}, \quad (42)$$

where λ is the reorganization energy and ω_c is the cut-off frequency. Note that the SPQME method cannot describe coherent dynamics for systems with this form of spectral density due to the infrared divergence problem in the small-polaron memory kernel. We also know that the most problematic parameter regime for the SPQME is at the slow-bath limit and weak system-bath couplings. Thus, we focus our study here in the weak system-bath coupling regime and choose to compare the FM-SPQME method with the Redfield theory. The Redfield theory is expected to yield accurate results in this regime. Note that in this work we aim to provide a proof-of-principle study to investigate the frozen mode approximation for the SPQME method in systems with the Drude-Lorentz spectral density, and a complete exploration of the validity of FM-SPQME for

the Drude-Lorentz model in full EET parameter space or comparisons to numerically exact methods (such as the HEOM approach) are outside the scope of this work. Furthermore, in this study, we choose to use an extremely small reorganization energy ($\lambda = 1$ cm^{-1}) to ensure the accuracy of the Redfield theory, and other parameters are set to imitate EET dynamics in photosynthetic light-harvesting systems.

Figure 5 shows population dynamics simulated by the FM-SPQME method and the Redfield theory for a model dimer system at a low temperature ($T = 77$ K) and different values of excitonic couplings. Following the results presented in Sec. III A, we also use variational ω_s [Eq. (31)] in the FM-SPQME calculations. Furthermore, since the original SPQME method cannot be utilized to calculate EET dynamics in this system because of the Drude-Lorentz spectral density, we present FM-SPQME results with a minuscule splitting frequency ($\omega_s = 0.1\omega_c$) to implicate the dynamics in a small-polaron theory. In addition, to examine a broad parameter range,

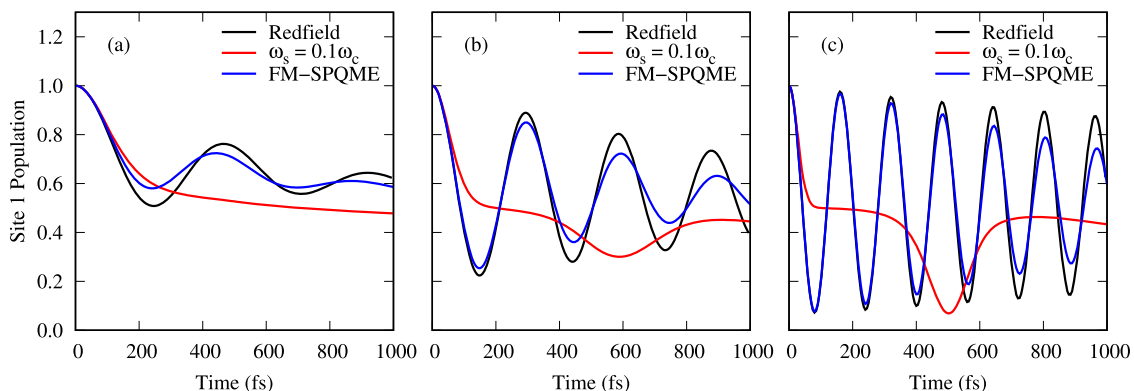


FIG. 6. Population dynamics simulated by the FM-SPQME method and the Redfield theory at a high temperature ($T = 300$ K) with different values of excitonic couplings: (a) $J = 25$ cm^{-1} , (b) $J = 50$ cm^{-1} , (c) $J = 100$ cm^{-1} . Other parameters are $\lambda = 1$ cm^{-1} , $\Delta = 25$ cm^{-1} , and $\omega_c = 50$ cm^{-1} . FM-SPQME splitting frequencies are (a) $\omega_s/\omega_c = 0.52$, (b) $\omega_s/\omega_c = 1.28$, (c) $\omega_s/\omega_c = 2.60$.

we vary J from the fast bath limit [Fig. 5(a)] to the slow bath limit [Fig. 5(c)] in this study. It is clear that the FM-SPQME with $\omega_s = 0.1J$ fails terribly in all parameters as long as the Drude-Lorentz spectral density is adopted. By contrast, the FM-SPQME with $\omega_s = J$ successfully captures the coherent dynamics even in the slow-bath limit [Fig. 5(c)].

In Fig. 6, we furnish high temperature results. Unphysical dynamics provided by the full small-polaron treatment are clearly observed in Fig. 6, and these unphysical results are caused by the infrared divergence problem in the small polaron formalism. The difficulty has also been revealed in previous studies.⁵⁴ On the other hand, the FM-SPQME approach still yields excellent results, demonstrating that the frozen-mode approximation circumvents problems caused by the low-frequency modes in the small-polaron framework. These results clearly show that with a small increase in the computational cost, the FM-SPQME method significantly extends the applicable regime of the SPQME into the slow-bath regime.

IV. CONCLUDING REMARKS

In order to expand the applicable regime of the small-polaron approach for EET dynamics in molecular aggregates, we propose a mixed quantum-classical representation to separate the bath modes into two parts. One mainly comprises the fast high-frequency modes and is treated with the small polaron quantum master equation. The other portion consists of slow low-frequency modes and is envisaged as dynamically arrested frozen modes that cause diagonal static disorder in the polaron transformed Hamiltonian. The separation is achieved by multiplying a splitting function onto the spectral density, with a splitting frequency ω_s to divide the two parts. Furthermore, we suggest using a variational approach to determine the splitting frequency. This leads to a frozen-mode SPQME method for quantum dynamics in molecular aggregates. We also note that the frozen-mode approach is related to a crude frequency dependent variational polaron theory.

To demonstrate the applicability of the FM-SPQME method, we compare EET dynamics calculated from the new method to numerically exact results for model dimer systems in a large parameter space. We show that the FM-SPQME formalism yields accurate EET dynamics for systems with the super-Ohmic spectral density in a large EET parameter space. Even in the slow-bath regime where the small polaron frame is not applicable, the combination of the frozen-mode approximation for the low-frequency vibrations and small polaron representation for the high-frequency modes adequately describes the coherent dynamics. Furthermore, the separated treatment of low-frequency modes further helps us to extend the applicability of the SPQME method to systems with a spectral density of the Ohmic form. We investigate the EET dynamics calculated from the FM-SPQME method for a model dimer system with a Drude-Lorentz spectral density in the weak system-bath coupling limit and then compare the results with those calculated from the Redfield theory. We demonstrate that the FM-SPQME method is applicable in this Ohmic form spectral density, avoiding the infrared divergence problem in the original SPQME. The success of the FM-SPQME method echoes a great physical insight that the difficulty in describing non-Markovian, multistep relaxation dynamics is the cause of failures in many perturbative methods, as have been emphasized by Reichman and co-workers.^{48–50}

This simple extension of the SPQME method significantly expands the applicability of the small-polaron approach and at the same time provides useful physical insights into the role of the low-frequency modes in the polaron representation. The success of the frozen-mode approximation indicates that the low-frequency part of the environmental modes does not dynamically modulate the EET dynamics. These modes remain “static” in the EET dynamics, providing only a Gaussian random energetic background in the ensemble. We believe this is a general principle in condensed-phase quantum dynamics, and it would be interesting to test this picture and its applicability in various systems spectroscopically, for example, using the photon echo spectroscopy. Notably, in a recent study, Fetherolf and Berkelbach⁶⁴ have demonstrated that the idea based on separate treatment of homogeneous and inhomogeneous spectral broadening enables accurate simulations of linear and nonlinear spectroscopy using perturbative second-order time-convolutionless quantum master equations.

Moreover, it is interesting to note that while various variational polaron methods also solve the slow-bath problems confronted in the SPQME,^{40,54,59} the FM-SPQME method retains the advantage of low computational cost and rapid convergence attributable to the frozen-mode approximation. In fact, simulations of quantum dynamics in molecular aggregate systems in condensed phases often require the inclusion of static disorders in site energies that lead to inhomogeneous broadening in spectra. Therefore, in such calculations, the sampling over thermalized phase space distribution for low-frequency modes in the FM-SPQME method posts no additional cost. Thus, we believe that the FM-SPQME method accomplishes accuracy and computational efficiency simultaneously. Finally, we emphasize that the utilization of the frozen-mode approximation in a polaronic framework is based on the physical insight that the adequacy of the fully dressed small polaron representation depends on the time scale of bath dynamics. Using the variationally determined splitting frequency, the frozen-mode method can be considered as a crude variational polaron theory with frequency-dependent polaronic dressing coefficient. The idea should not be limited to descriptions of EET dynamics, and it should be fruitful to extend the FM-SPQME method to treat charge mobility as well as charge separation processes in a broad range of biological and chemical systems. Further improvement of the FM-SPQME method such as a better determination of the splitting frequency for general bath spectral densities, generalization to treat charge-mobility problems, and a more comprehensive benchmark in the case of Ohmic spectral density is a worthy path to pursue.

ACKNOWLEDGMENTS

Y.-C.C. thanks the Ministry of Science and Technology, Taiwan (Grant No. MOST 105-2113-M-002-012), National Taiwan University (Grant No. 103R891305), and Center for Quantum Science and Engineering (Subproject No. 103R891401) for financial support. H.-H.T. and B.-Y.J. acknowledge the financial support from the Ministry of Science and Technology, Taiwan (Grant No. NSC 105-2628-M-002-012). We are grateful to Computer and Information Networking Center, National Taiwan University, for the support of high-performance computing facilities. We are grateful to the National Center for High-performance Computing for computer time and facilities.

REFERENCES

- ¹P. F. Barbara, A. J. Gesquiere, S.-J. Park, and Y. J. Lee, *Acc. Chem. Res.* **38**, 602 (2005).
- ²I. Burghardt, V. May, D. A. Micha, and E. R. Bittner, *Energy Transfer Dynamics in Biomaterial Systems* (Springer, 2009).
- ³I. Hwang and G. D. Scholes, *Chem. Mater.* **23**, 610 (2011).
- ⁴G. D. Scholes and G. Rumbles, *Nat. Mater.* **5**, 683 (2006).
- ⁵T. Renger, V. May, and O. Kühn, *Phys. Rep.* **343**, 137 (2001).
- ⁶Y.-C. Cheng and G. R. Fleming, *Annu. Rev. Phys. Chem.* **60**, 241 (2009).
- ⁷V. May and O. Kühn, *Charge and Energy Transfer Dynamics in Molecular Systems* (Wiley VCH, 2011).
- ⁸S. Yang, D. Z. Xu, Z. Song, and C. P. Sun, *J. Chem. Phys.* **132**, 234501 (2010).
- ⁹T. Scholak, F. de Melo, T. Wellens, F. Mintert, and A. Buchleitner, *Phys. Rev. E* **83**, 021912 (2011).
- ¹⁰Q. Ai, T.-C. Yen, B.-Y. Jin, and Y.-C. Cheng, *J. Phys. Chem. Lett.* **4**, 2577 (2013).
- ¹¹T. Renger, A. Klinger, F. Steinecker, M. Schmidt, J. Numata, and F. Müh, *J. Phys. Chem. B* **116**, 14565 (2012).
- ¹²F. Fassio, R. Dinshaw, P. C. Arpin, and G. D. Scholes, *J. R. Soc., Interface* **11**, 20130901 (2013).
- ¹³S. Chandrasekaran, M. Aghtar, S. Valleeau, A. Aspuru-Guzik, and U. Kleinekathöfer, *J. Phys. Chem. B* **119**, 9995 (2015).
- ¹⁴J. M. Moix, Y. Zhao, and J. Cao, *Phys. Rev. B* **85**, 115412 (2012).
- ¹⁵U. Schollwöck, *Rev. Mod. Phys.* **77**, 259 (2005).
- ¹⁶J. Prior, A. W. Chin, S. F. Huelga, and M. B. Plenio, *Phys. Rev. Lett.* **105**, 050404 (2010).
- ¹⁷Y. Tanimura and R. Kubo, *J. Phys. Soc. Jpn.* **58**, 101 (1989).
- ¹⁸Y. Tanimura, *J. Phys. Soc. Jpn.* **75**, 082001 (2006).
- ¹⁹A. Ishizaki and G. R. Fleming, *J. Chem. Phys.* **130**, 234111 (2009).
- ²⁰J. Jin, X. Zheng, and Y. Yan, *J. Chem. Phys.* **128**, 234703 (2008).
- ²¹G. Tao and W. H. Miller, *J. Phys. Chem. Lett.* **1**, 891 (2010).
- ²²P. Huo, T. F. Miller III, and D. F. Coker, *J. Chem. Phys.* **139**, 151103 (2013).
- ²³M. K. Lee, P. Huo, and D. F. Coker, *Annu. Rev. Phys. Chem.* **67**, 639 (2016).
- ²⁴N. Makri, *Comput. Phys. Commun.* **63**, 389 (1991).
- ²⁵R. Kapral, *Annu. Rev. Phys. Chem.* **57**, 129 (2006).
- ²⁶R. Kapral and G. Ciccotti, *J. Chem. Phys.* **110**, 8919 (1999).
- ²⁷S. Bai, W. Xie, and Q. Shi, *J. Phys. Chem. A* **118**, 9262 (2014).
- ²⁸A. G. Redfield, *IBM J. Res. Dev.* **1**, 19 (1957).
- ²⁹W. T. Pollard, A. K. Felts, and R. A. Friesner, *Adv. Chem. Phys.* **93**, 77 (1996).
- ³⁰V. T. Förster, *Ann. Phys.* **437**, 55 (1948).
- ³¹R. van Grondelle and V. I. Novoderezhkin, *Phys. Chem. Chem. Phys.* **8**, 793 (2006).
- ³²A. Olaya-Castro and G. D. Scholes, *Int. Rev. Phys. Chem.* **30**, 49 (2011).
- ³³M. Schröter, S. Ivanov, J. Schulze, S. Polyutov, Y. Yan, T. Pullerits, and O. Kühn, *Phys. Rep.* **567**, 1 (2015).
- ³⁴W. M. Zhang, T. Meier, V. Chernyak, and S. Mukamel, *J. Chem. Phys.* **108**, 7763 (1998).
- ³⁵M. Yang and G. R. Fleming, *Chem. Phys.* **282**, 163 (2002).
- ³⁶S. Jang and Y.-C. Cheng, *Wiley Interdiscip. Rev.: Comput. Mol. Sci.* **3**, 84 (2013).
- ³⁷Y.-H. Hwang-Fu, W. Chen, and Y.-C. Cheng, *Chem. Phys.* **447**, 46 (2015).
- ³⁸Y. Chang and Y.-C. Cheng, *J. Chem. Phys.* **142**, 034109 (2015).
- ³⁹A. Ishizaki and G. R. Fleming, *J. Chem. Phys.* **130**, 234110 (2009).
- ⁴⁰C. K. Lee, J. Moix, and J. Cao, *J. Chem. Phys.* **136**, 204120 (2012).
- ⁴¹H.-T. Chang, P.-P. Zhang, and Y.-C. Cheng, *J. Chem. Phys.* **139**, 224112 (2013).
- ⁴²S. Jang, *J. Chem. Phys.* **131**, 164101 (2009).
- ⁴³A. Nazir, *Phys. Rev. Lett.* **103**, 146404 (2009).
- ⁴⁴S. Jang, *J. Chem. Phys.* **135**, 034105 (2011).
- ⁴⁵D. P. S. McCutcheon and A. Nazir, *Phys. Rev. B* **83**, 165101 (2011).
- ⁴⁶A. Kolli, A. Nazir, and A. Olaya-Castro, *J. Chem. Phys.* **135**, 154112 (2011).
- ⁴⁷H. Wang, M. Thoss, and W. H. Miller, *J. Chem. Phys.* **115**, 2979 (2001).
- ⁴⁸T. C. Berkelbach, D. R. Reichman, and T. E. Markland, *J. Chem. Phys.* **136**, 034113 (2012).
- ⁴⁹T. C. Berkelbach, T. E. Markland, and D. R. Reichman, *J. Chem. Phys.* **136**, 084104 (2012).
- ⁵⁰A. Montoya-Castillo, T. C. Berkelbach, and D. R. Reichman, *J. Chem. Phys.* **143**, 194108 (2015).
- ⁵¹N. Makri and D. E. Makarov, *J. Chem. Phys.* **102**, 4600 (1995).
- ⁵²N. Makri and D. E. Makarov, *J. Chem. Phys.* **102**, 4611 (1995).
- ⁵³H.-T. Chang and Y.-C. Cheng, *J. Chem. Phys.* **137**, 165103 (2012).
- ⁵⁴D. P. S. McCutcheon and A. Nazir, *J. Chem. Phys.* **135**, 114501 (2011).
- ⁵⁵D. R. Yarkony and R. J. Silbey, *J. Chem. Phys.* **67**, 5818 (1977).
- ⁵⁶T. Harris and R. J. Silbey, *J. Chem. Phys.* **83**, 1069 (1985).
- ⁵⁷A. H. Romero, D. W. Brown, and K. Lindenberg, *Phys. Rev. B* **59**, 13728 (1999).
- ⁵⁸Y.-C. Cheng and R. J. Silbey, *J. Chem. Phys.* **128**, 114713 (2008).
- ⁵⁹F. A. Pollock, D. P. S. McCutcheon, B. W. Lovett, E. M. Gauger, and A. Nazir, *New J. Phys.* **15**, 075018 (2013).
- ⁶⁰A. Nazir, D. P. S. McCutcheon, and A. W. Chin, *Phys. Rev. B* **85**, 224301 (2012).
- ⁶¹Y. Fujihashi and A. Kimura, *J. Phys. Chem. B* **119**, 8349 (2015).
- ⁶²H. Wang, X. Song, D. Chandler, and W. H. Miller, *J. Chem. Phys.* **110**, 4828 (1999).
- ⁶³J. Eckel, S. Weiss, and M. Thorwart, *Eur. Phys. J. B* **53**, 91 (2006).
- ⁶⁴J. H. Fetherolf and T. C. Berkelbach, *J. Chem. Phys.* **147**, 244109 (2017).